Noncovalent Self-Assembled Monolayers on Graphene as a Highly Stable Platform for Molecular Tunnel Junctions

*Peng Song, C. S. Suchand Sangeeth, Damien Thompson, Wei Du, Kian Ping Loh, and Christian A. Nijhuis**

Molecular electronic junctions based on self-assembled monolayers (SAMs) are often based on SAMs of organothiolates supported by noble metal surfaces (usually Au or Ag) in contact with a top electrode.[1–4] The organothiolate-metal chemistry yields high-quality SAMs and is therefore useful to incorporate in junctions, but the metal—thiolate bond is unstable in ambient conditions and readily decomposes,[5] and the number of stable thiols is limited (thiols decompose in ambient conditions to their disulfide analogs).[5] Monolayers that are immobilized on surfaces via covalent chemistry (such as those formed on Si,[6] Al/AlO_x,[7] or pyrolyzed photoresist film,[8,9] and their corresponding junctions, are stable, but the formation process lacks the reversible character that is required in a self-assembly process that relies on self-repair and yields monolayers that are less densely packed and more defective than their metal—thiolate SAM analogs.[5,10]

Here, we report a tunnel junction based on noncovalent SAMs of alkylamines $(H_2N(CH_2)_{n-1}CH_3$ or H_2NC_n with n = 8, 10, 12, 14, or 16) on monolayer graphene supported by Cu. To form electrical contacts to the SAMs in a noninvasive manner, we used the EGaIn technique (see the Supporting Information for more details). This technique relies on a moldable non-Newtonian liquid[3,11] of GaO_x^{cond}/EGaIn, where GaO_x^{cond} is a 0.7 nm thick native layer of a highly conductive oxide[12,13] and EGaIn denotes the eutectic alloy of Ga and In. It can be molded into cone-shaped tips (with a tip radius of 20–30 μm) suspended from a syringe (mounted on a micromanipulator),[14,15] or stabilized in microfluidic channels,[3,16] which are brought in contact with the SAMs. The soft character of this material ensures the formation of good electrical contacts with the SAMs without causing damage. Once the contacts have been made, the top-electrode material behaves as if it were a solid because of its non-Newtonian nature to yield stable junctions. The cone-shaped top electrodes enable us to collect large number data sets conveniently in an ordinary laboratory. The microfluidic top electrodes are more laborious to fabricate than the cone-shaped tips, but their good mechanical stability and well-defined geometrical contact area enables to conduct impedance, $J(V,T)$, and stability measurements. Hence, in this study we used both methods to form junctions and we clearly state in the figure legends which of the two methods was used to generate each dataset.

The junctions are abbreviated as Cu//Graphene//H_2NC_n//GaO_x^{cond}/EGaIn, where "//" denotes a noncovalent contact and "/" the interface of the GaO_x with the bulk liquid metal alloy.[17] **Figure 1** shows the schematic illustration of the tunnel junctions. We used graphene grown on Cu by chemical vapor deposition (CVD) because graphene is chemically stable up to 500 °C in air,[18] highly conductive, and wafer-scale CVD graphene is available.[19] The H_2NC_n precursors form densely packed SAMs on graphene because the noncovalent amine–graphene interactions allow for self-repair at the molecular scale,[20,21] and as we show here, these SAMs do not suffer from the chemical instability inherent to organothiolate SAMs. Unlike previously reported methods to form graphene-monolayer-based tunnel junctions using covalent chemistry,[22] the van der Waals interaction of the amine moieties with graphene does not damage the chemical structure of graphene, i.e., it does not change the sp^2 hybridization of the carbon network and the reversible nature of the graphene–amine interaction makes self-repair possible resulting in good tunneling barriers (i.e., a tunneling decay coefficient of $1.02 \pm 0.08\ n_C^{-1}$). Junctions with covalent monolayers on graphene do not form good tunneling barriers (i.e., the tunneling decay coefficient of $\approx 0.67\ n_C^{-1}$ is low)[26] likely because of low packing densities and defects[6] as a result of a lack of self-repair during the assembly process as explained above (see also section Molecular length dependent charge transport). In addition, the graphene layer itself effectively blocks ambient oxygen from oxidizing the underlying Cu substrate.[23,24]

We characterized the two-terminal devices with both AC and DC techniques from which we conclude that the electrical characteristics are dominated by the molecular properties of the junctions and the mechanism of charge transport across the junction is coherent tunneling. The junctions can be fabricated with good yields in nonshorting junctions of 93% and

P. Song, Dr. C. S. S. Sangeeth, W. Du, Prof. K. P. Loh, Prof. C. A. Nijhuis
Department of Chemistry
National University of Singapore
3 Science Drive 3
Singapore 117543, Singapore
E-mail: chmnca@nus.edu.sg

P. Song, Dr. C. S. S. Sangeeth, W. Du, Prof. K. P. Loh, Prof. C. A. Nijhuis
Centre for Advanced 2D Materials and Graphene Research Centre
National University of Singapore
6 Science Drive 2
Singapore 117546, Singapore

Dr. D. Thompson
Materials and Surface Science Institute and Department of Physics and Energy
University of Limerick
Co. Limerick, Ireland

DOI: 10.1002/adma.201504207

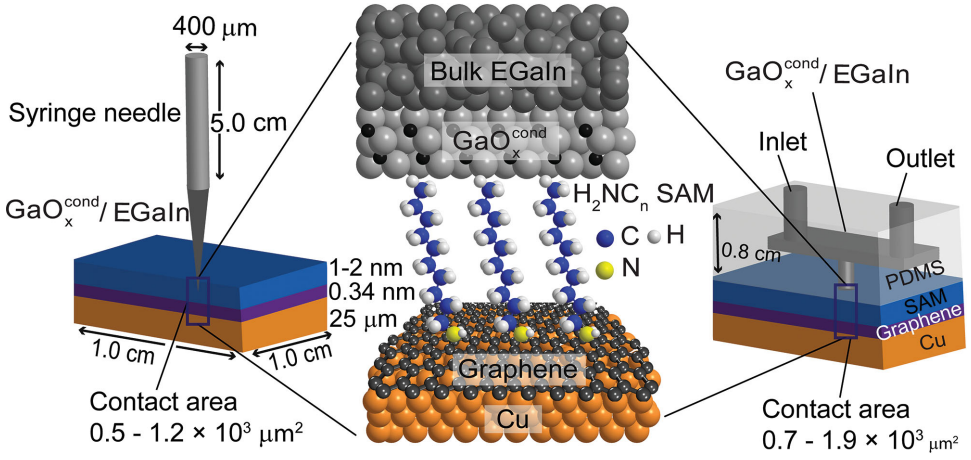

Figure 1. Schematic illustrations of the tunnel junction. The structure of the Cu//Graphene//H_2NC_n// GaO_x^{cond} /EGaIn tunnel junction. Two different types of top electrodes are used as indicated in the main text. The left panel shows the junction with the cone-shaped top electrode. The right panel shows the microfluidic cell with the top electrode stabilized in PDMS; not drawn to scale.

the contact resistance is negligible. We also found that the junctions are electrically stable against voltage cycling (N = 1200 cycles), continuous biasing (retain currents for 100 000 s at –1.0 V), and aging in ambient conditions (room temperature; relative humidity: 60%–65%) for more than 30 d. Our demonstrated device stabilities and electrical characteristics show that graphene is a promising bottom electrode material to fabricate SAM-based tunnel junctions. We believe that this platform is useful for future physical-organic studies of charge transport at the molecular scale.

SAM Characterization: We formed CVD monolayer graphene on Cu using previously reported methods.[19] On this graphene, we formed the SAMs of H_2NC_n following a method reported by Long et al.[20] that we scaled up from exfoliated graphene flakes of a few tens of micrometers in diameter to large-area (wafer-scale) CVD graphene. By using graphene on Cu immediately after the CVD process, we minimized contamination from the ambient and the graphene is free from impurities, such as residual polymers, associated with transferred graphene.[24,25] To characterize the graphene by Raman spectroscopy, we transferred the graphene to Si/SiO_2 (with an oxide layer thickness of 300 nm) because of the high background signals of Cu. **Figure 2**a shows that the D band (1344 cm^{-1}) associated with defects is weak, the intensity ratio between 2D and G band is 2.7 ± 0.3, and the full width at half maximum (FWHM) of the 2D peak is 31.6 ± 0.9 cm^{-1}. These values agree well with previously reported values for monolayer CVD graphene with largely maintained sp^2 hybridization and minimal defects.[26] The Raman spectra together with the atomic force microscopy data (AFM; see Figure S2a,b in the Supporting Information) show that the we have continuous monolayer graphene with good quality (some residual polymer that was used in the transfer process is visible; this residual polymer is not present on the Cu//Graphene samples). The Cu//Graphene substrate shows large grains (with root mean square roughness of 0.87 nm; see Figure S2c–f in the Supporting Information), which are beneficial for fabrication of junctions.

The SAMs cause three spectral changes in the Raman spectra (see Figure 2a) that are consistent with charge transfer doping and the noncovalent nature of the amine–graphene interaction. The intensity of the D band does not increase as expected for noncovalent interactions, the position of the G band shifts to higher energy by 7.2 ± 0.1 cm^{-1}, which corresponds to a Fermi level shift of 0.17 eV (G band shift $\Delta\Omega_G = |\Delta E_F| \times 42\ cm^{-1}\ eV^{-1}$),[27] and the intensity ratio of the 2D and G bands decreases by a factor of ≈2.[20,28]

Fourier transform infrared reflection absorption spectroscopy (FTIRAS) has been widely used to study the structure of SAMs on metal surfaces.[29–32] Briefly, only the vibrational transition dipole moment in the direction perpendicular to surface contributes to the IR absorption spectra and the structure of the SAM can be determined by comparing observed peak frequencies with reference data.[29] Figure 2b shows the IR absorption spectra of the H_2NC_n SAMs with n = 8, 10, 12, 14, and 16. The IR spectra show three distinct vibrational modes associated with alkyl chains at 2926 cm^{-1} (the asymmetric stretching mode of —CH_3), 2923 cm^{-1} (asymmetric stretching mode of —CH_2—), and 2850 cm^{-1} (symmetric stretching mode of —CH_2—). These frequencies are close to values observed for densely packed SAMs of alkylamines on quartz[31] and mica,[32] where the interaction strength between the SAM and substrate is well below a well-defined covalent bond. The frequencies of the two stretching modes of —CH_2— also indicate a largely all-trans orientation of alkyl chains in the SAMs, indicative of a close-packed, ordered SAM.[33] Together with the Raman spectra, FTIRAS proves the formation of ordered SAMs on graphene.

To understand the structures of the SAMs supported by graphene in more detail, we used molecular dynamics to quantify the atomic-scale structure, dynamics and energetics of the SAM–graphene interface and the SAM packing structure. Figure 2c–h shows the computed SAM structures on graphene for n = 8, 12, and 16. The amine group in the molecule anchors on graphene due to physisorption and the alkylamine molecules self-assemble into upright monolayers. As suggested in

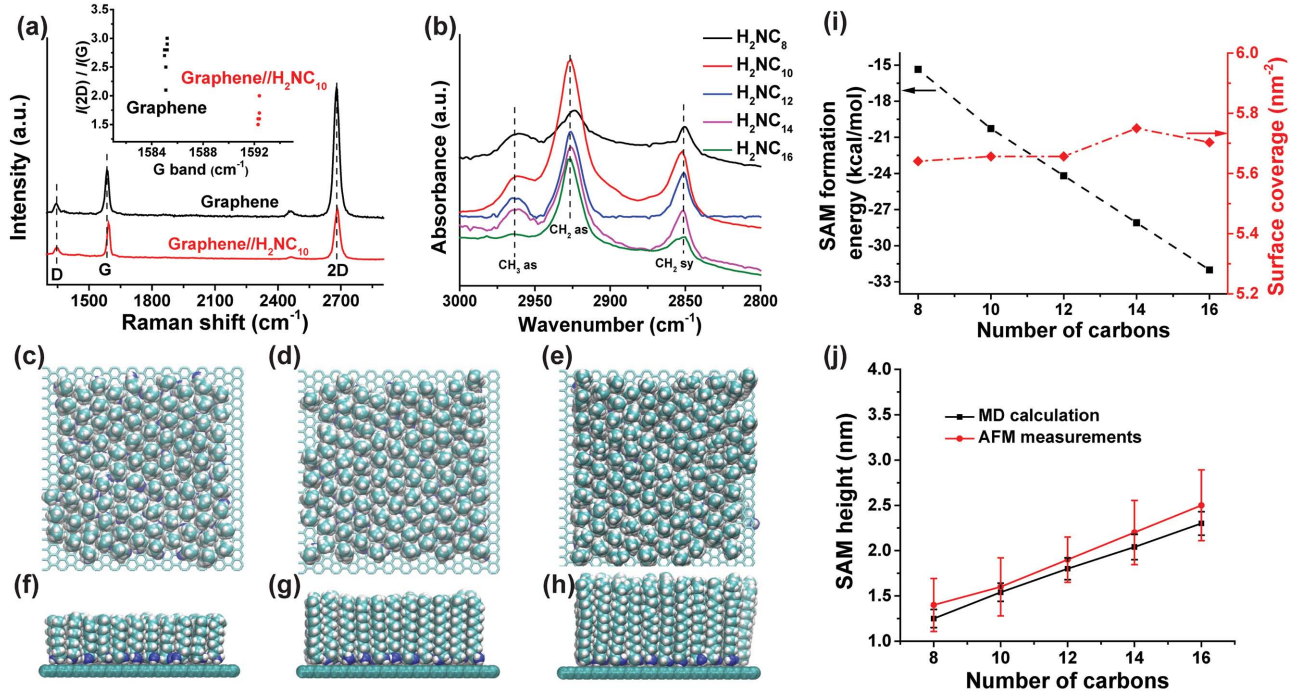

Figure 2. Characterization of the H_2NC_n SAMs on graphene. a) The Raman spectra of graphene transferred from Cu to SiO_2 before and after growth of a H_2NC_{10} SAM (the inset shows the G peak positions and I_{2D}/I_G ratios of ten randomly selected spots (spot size: 1 μm^2) for each sample (note that some data points are overlapping). b) The IR absorption spectra of H_2NC_n SAMs with n = 8, 10, 12, 14, and 16, formed on freshly prepared CVD graphene on Cu. c–e) Top and f–h) side views of the calculated SAM structures of H_2NC_8, H_2NC_{12}, and H_2NC_{16} on graphene, respectively. The full simulation cells each contain 784 H_2NC_n molecules assembled on a 13 × 15 nm^2 graphene sheet, as described in Methods. i) The SAM formation energies and surface coverages as a function of n. Errors on these data points are 0.6–1.1 kcal mol^{-1} and 0.04–0.06 molecules nm^{-2}, respectively, estimated as standard deviations summed over molecule-, time- and n-averaged structures. j) The SAM heights derived from MD calculations (errors bars represent the same standard deviation as panel i) and AFM measurements (error bars represent the standard deviation of the height distributions, see Figure S3 in the Supporting Information) as a function of n.

previous calculations, the binding interactions between graphene and alkylamine molecules are dominated by noncovalent van der Waals forces.[20,21] Molecular dynamics also improve the quantitative understanding about SAM packing energies and density which we relate to the stability of the junctions and the film heights of the SAMs which help to establish the mechanism of charge transport and the capacitance of the SAMs (see below).[15] Figure 2i shows that the alkylamines form SAMs on graphene with a surface coverage of about 5.7 molecules nm^{-2}, indicating densely packed SAMs on graphene. Figure 2j shows that the SAM heights derived from MD range from 1.2 to 2.4 nm as n increases from 8 to 16 which are within experimental error of the values measured by AFM (see Figure S3 for the AFM images in the Supporting Information) which further validates the MD models. The AFM images also show that the alkylamines form continuous films which are consistent with previous observations.[20] The SAM formation energy (packing energy plus the SAM-substrate interaction) increases by about 2.1 kcal mol^{-1} per additional CH_2 unit. We found, both from experiment and theory, that no stable SAMs formed when $n \leq 6$ (but we did not investigate SAMs on graphene for $n > 16$). These SAMs only form stable structures when the SAM packing energies exceeds 15 kcal mol^{-1}, which is similar to that found in noncovalent biological systems such as bilayer lipids that form cell membranes.[34] For instance, alkylcarboxylic acids with chain lengths shorter than eight carbons cannot form vesicles.[35]

Molecular Length-Dependent Charge Transport: To determine the charge transport characteristics across the junctions, we recorded statistically large numbers of $J(V)$ curves (0 → +1.0 V → −1.0 V → 0 in steps of 50 mV; in total we used 2539 traces in this study) with cone-shaped GaO_x^{cond}/EGaIn top electrodes. For each type of SAM, we formed 20–26 junctions on 2–3 different substrates and recorded 20 $J(V)$ curves for each individual junction and 467–625 traces for each type of junction (see Table S1 in the Supporting Information). **Figure 3**a shows the $J(V)$ traces (each data point is the Gaussian mean of the values of $\log_{10}|J|$ or $\langle\log_{10}|J|\rangle_G$, determined at a given applied voltage) of the junction as a function of n. We consider the $J(V)$ curves to be practically symmetrical as the values of $\langle\log_{10}|J|\rangle_G$ at positive biases are only slightly higher (by less than a factor of 2) than those values of $\langle\log_{10}|J|\rangle_G$ at the corresponding negative bias; this small asymmetry in the $J(V)$ curves is likely caused by the work function difference between GaO_x^{cond}/EGaIn (4.3 eV)[15] and graphene (4.5 eV)[36] and other asymmetries in the junction. Statistical analysis of the charge transport data for each junction is discussed in detail in the Supporting Information and uses previously reported methods.[37]

Simmons derived a theory to model the tunneling current density though rectangular tunneling barriers. In the low-bias regime, the simplified version of the Simmons equation can be written as Equation (1), where β is the tunneling decay constant (in Å^{-1} or n_C^{-1}), d (in Å or n_C) is the barrier width, V (in V)

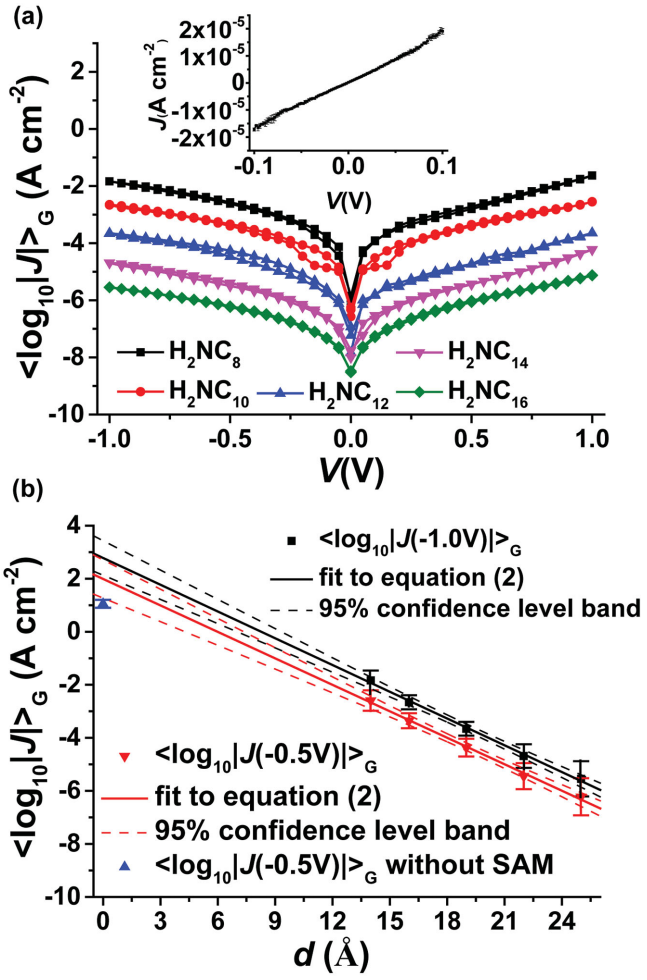

Figure 3. Charge transport through SAMs on graphene measured with cone-shaped top electrodes. a) Semilog plots of the current density versus applied bias of Cu//Graphene//H_2NC_n// GaO_x^{cond} /EGaIn with n = 8, 10, 12, 14, and 16. The inset shows the $J(V)$ characteristics in the low-bias regime for a junction with H_2NC_{10} SAM. b) Semilog plots of the value of $|J|$ determined at –1.0 and –0.5 V versus d (obtained from AFM measurements) with the corresponding fit to Equation (2) and 95% confidence level bands. The error bars represent standard deviation of $\log_{10}|J|$ of each junction.

is the applied bias, J (in A cm^{-2}) is the current density that flows through the barrier, and J_0 (in A cm^{-2}) is the hypothetical current density that flows across the junctions when d is zero. It shows that the $J(V)$ curves should be linear in the low-bias regime. While in the high-bias regime, this simplified equation does not hold as is apparent from the nonlinear character of the $J(V)$ curves in this so-called high-bias regime and the full form of the Simmons equation should be used (not shown). The $J(V)$ curves are nonlinear in the high-bias regime and the inset of Figure 3a shows the linear behavior in the low-bias regime (–0.10 to 0.10 V) for a junction with a SAM of H_2NC_{10}, as expected when tunneling is the dominant mechanism of charge transport.

$$J = J_0 / dV e^{-\beta d} \quad (1)$$

$$J = J_0 e^{-\beta d} \quad (2)$$

The Simmons equation is usually further simplified to Equation (2) (all symbols have the same meaning as in Equation (1)), the general tunneling equation, to obtain the values of β and J_0 from a plot of the measured value of J against d which were obtained from the MD data (Figure 2j). We fitted Equation (2) by minimizing the error of the least squares and the values of $\langle\log_{10}|J|\rangle_G$ and assuming that the data are normally distributed (method 1), or by minimizing the sum of the absolute values of the error of all $\log_{10}|J|$ without making assumptions regarding the nature of distribution of the data[37] (method 2). Figure 3b shows the value of $\langle\log_{10}|J|\rangle_G$ for junctions with n = 8, 10, 12, 14, and 16, recorded at–1.0 V with a fit to Equation (2) using method 1. The fit with method 2 is shown in Figure S6, Supporting Information. Both methods yield indistinguishable values of β and J_0 from which we concluded that the data are normally distributed. We use the results obtained by method 1 in the remainder of this article and the error bars of the values of J, β, and J_0 represent the 95% confidence intervals. In our analysis we used values of J determined at negative biases, but considering the symmetry of the $J(V)$ curves, we note that the same analysis at positive bias would result in the same conclusions. To show the robustness of our analysis, Figure S5 (Supporting Information) plots the same relations as Figure 3b but using J values determined at +0.5 and +1.0 V.

The value of $\log_{10}|J_0|$ at –1.0 V is 2.8 ± 0.8 A cm^{-2}. The value of $\log_{10}|J_0|$ at –0.5 V is 2.0 ± 0.9 A cm^{-2}, which is a factor of 3–5 lower than J_0 values obtained for Ag^{TS}-SC_n// GaO_x^{cond}/EGaIn junctions (where Ag^{TS} = template-stripped silver) at the same voltage,[3,38,39] for reasons discussed below.

We also measured the $J(V)$ curves of junctions without SAM, i.e., Cu//Graphene// GaO_x^{cond}/EGaIn (see Figure S7 in the Supporting Information), and the current flow across this junction can be used to estimate the value of J_0 as d is zero in this case. At –0.5 V, the value of $\langle\log_{10}|J|\rangle$ for junction without SAM is 1.1 ± 0.2 A cm^{-2}, which falls in the 95% confidence level of the extrapolated value of J_0 at –0.5 V based on Equation (2). This observation validates the extrapolation of the data back to d = 0.[39]

The value of β is related to the height and shape of the tunneling barrier imposed by the SAMs and the nature of the SAM-electrode contact. For junctions with aliphatic SAMs, the empirical consensus value of β = 0.9–1.1 n_C^{-1} seems to apply for a large number of test-beds and is associated with coherent through-bond tunneling.[2,14,16,40] We determined a value of β = 0.82 ± 0.18 Å^{-1}, or equivalently 1.02 ± 0.08 n_C^{-1}, and we show below that the $J(V)$ curves are independent over a broad range of temperature of 100–340 K. These results indicate that the mechanism of charge transport across junctions of Cu//Graphene//H_2NC_n// GaO_x^{cond} /EGaIn is coherent through-bond tunneling.[12,41,42]

The value of β is also an indicator of the quality of SAM-based junctions, along with the yields in working junctions, the values of σ_{log} and the values of J_0.[3] Crucially, defects lower or increase the observed value of β. We showed that defects in metallic bottom electrodes can decrease the value of β to as low as 0.41 n_C^{-1} because defects lower the effective thickness of the SAMs and therefore the assumption $d = n_c$ is not valid.[4] Values of $\beta > 1.0\ n_C^{-1}$ are indicative of defective SAMs and Slowinski et al.

proposed that in such junctions chain-to-chain tunneling is important.[42] Others proposed that the presence of pinholes,[7] electrostriction,[43] and the force the top electrode exerts on the SAM (in conductive probe experiments) can all alter the value of β.[44] For similar reasons, the value of J_0 is sensitive to defects, and we showed that defects on silver substrates increase (up to a factor of 10^3) or lower (up to a factor of 10^2) the measured value of J_0 in *n*-alkanethiolate SAMs.[38] The value of β obtained for the Cu//Graphene//H_2NC_n// GaO_x^{cond}/EGaIn junctions falls in the range of consensus values, the yields in working junctions are high (90%–95%), and we found small values of σ_{log} of 0.27–0.70 (see Table S1 in the Supporting Information). Thus we conclude that our junctions are of good quality and that their charge transport characteristics are dominated by the supramolecular structure of the SAMs.

Impedance Measurements: The impedance Z is a more general form of resistance and includes, unlike resistance R, both the magnitude and phase (see the Supporting Information for background details on impedance spectroscopy). For instance, ideal resistors have a zero phase angle (i.e., $\phi = 0°$) and the value of Z is independent of the applied frequency. In contrast, a frequency dependent resistance, the so-called capacitive reactance $X_c = 1/\omega C_{SAM}$, where ω (in rad s^{-1}) is the frequency of the AC signal, is caused by a capacitor which has, in principle, a value of $\phi = 90°$.[45] Thus, by subjecting a circuit to an AC signal with varying frequency while measuring the impedance one can determine the circuit elements that impede charge transport independently from each other.

We showed that impedance spectroscopy gives complementary information to DC $J(V)$ measurements regarding the electrical characteristics of alkanethiolate SAM-based junctions on silver.[12] For the impedance measurements, we used PDMS confined microfluidic GaO_x^{cond}/EGaIn electrodes that were stabilized in a microfluidic through-hole in a transparent rubber of polydimethylsiloxane (PDMS; see Figure S1 in the Supporting Information). We measured the impedance spectra of the Cu//Graphene//H_2NC_n// GaO_x^{cond}/EGaIn junctions at zero bias using a sinusoidal signal with an amplitude of 30 mV in the frequency range of 1 Hz to 1 MHz by following previously reported procedures.[12] **Figure 4**a shows the frequency dependence of the modulus of the complex impedance $|Z|$. The data were fitted using the equivalent circuit shown in the inset of Figure 4a. An ideal capacitor has a phase angle $\phi = 90°$ at high frequencies (Figure S11a, Supporting Information) and appears in a Nyquist plot (a plot of the imaginary part (Z'') against the real part (Z') of the impedance) as a semicircle (Figure S11b,c, Supporting Information). In our case, the contact resistance R_C consists of the resistance of the SAM-top electrode contact ($R_{C,t}$) and SAM-bottom electrode contact ($R_{C,b}$), resistance of the GaO_x^{cond} layer, resistance of the GaO_x^{cond} //SAM noncovalent

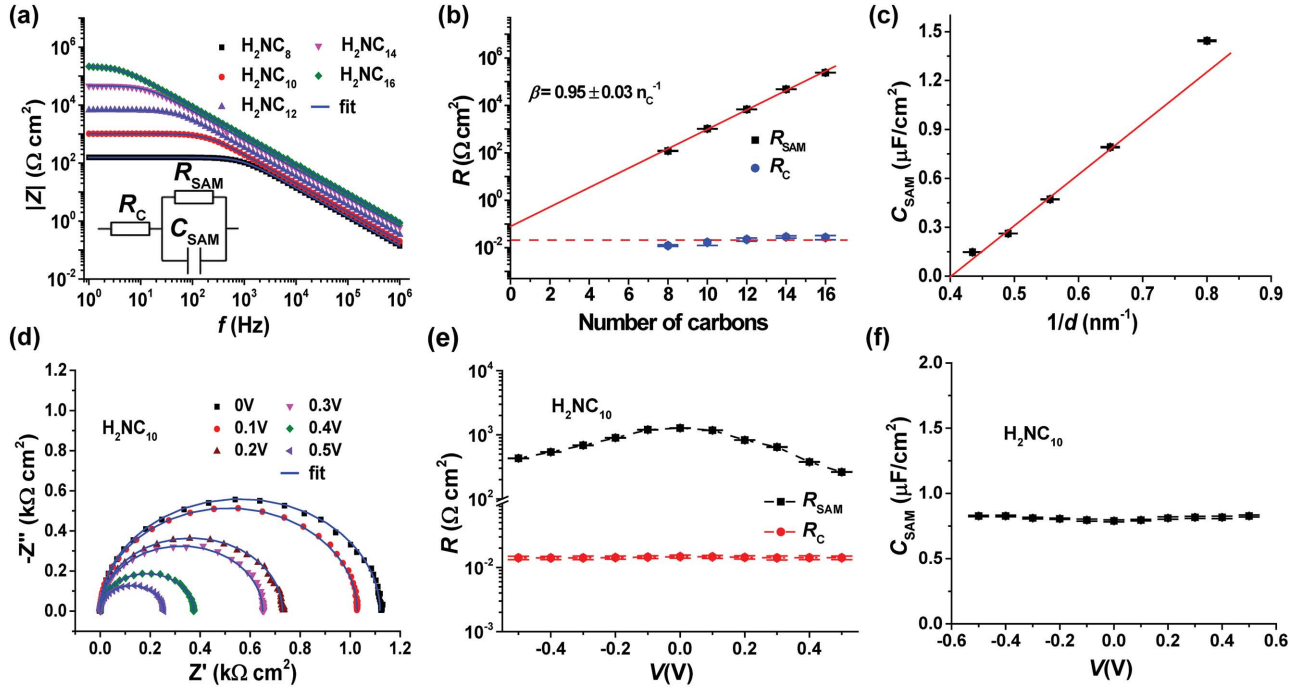

Figure 4. Impedance spectroscopy of the junctions on graphene measured with PDMS confined microfluidic top electrodes. a) The frequency dependency of modulus of complex impedance of the junctions with SAMs of $n = 8$, 10, 12, 14, or 16 with the fits (solid lines) to the equivalent circuit shown in the inset. b) The value of R_{SAM} and R_C as a function of n (the red solid line is a fit to Equation (5) and the red dashed line is a guide to the eye), c) the value of C_{SAM} as a function of $1/d$ (the d was obtained by AFM). Bias dependent d) Nyquist plots and fits to equivalent circuit of junction with SAM of H_2NC_{10} at different DC in the bias range of ±0.50 V measured at intervals of 0.10 V and the corresponding e) R_{SAM}, R_C and f) C_{SAM} as function of applied bias. All impedance data were validated with the KK test (see the Supporting Information), i.e., the data are linear and the system was in thermodynamic equilibrium (see Figures S9 and S11 for KK residual plots in the Supporting Information). The values of χ^2_{KK} fall in the range of $1.0–1.7 \times 10^{-3}$ (see Tables S2 and S3 in the Supporting Information), which we attribute to noise. The data fitted well to the equivalent circuit shown in the inset of (a) (see Figures S10 and S12 for the residual plots in the Supporting Information). The values of χ^2_{fit} fall in the range of $1.2–2.0 \times 10^{-3}$ (see Tables S2 and S3 in the Supporting Information) which are similar to the range of χ^2_{KK} values.

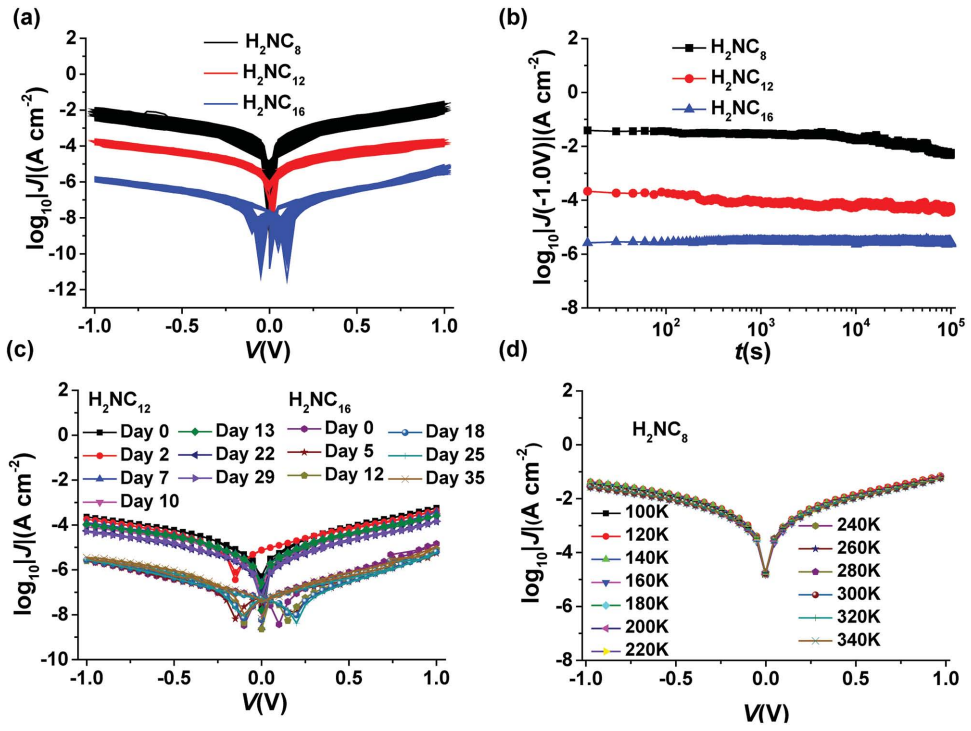

Figure 5. Stability tests of the junctions measured with PDMS confined microfluidic top electrodes. a) 1200 cycles $J(V)$ curves for junctions with SAMs of H_2NC_8, H_2NC_{12}, and H_2NC_{16}. b) Retention characteristics of junctions with SAMs of H_2NC_8, H_2NC_{12}, and H_2NC_{16} at constant bias of –1.0 V (the current was sampled at intervals of 15 s). c) The $J(V)$ characteristics of junctions of H_2NC_{12} and H_2NC_{16} monitored for a period of time of 29 or 35 d in ambient conditions (60%–65% relative humidity at 298 K). d) The $J(V)$ characteristics of a junction with SAMs of H_2NC_8 as a function of temperature ranging from 100 to 340 K measured at intervals of 10 K (data are plotted for every 20 K for clarity, the complete data set is shown in Figure S14d, Supporting Information).

interface and resistance of the Graphene//SAM interface and Cu//Graphene interface.

The equivalent circuit can be understood using the Landauer formalism (see for details ref. [46]). The total resistance of a molecular tunnel junction ($R_{junction}$) is given by Equation (3), where h is the Planck's constant, e is the charge of an electron, T is the transmission probability, M is the number of conduction channels (which we believe is 1 for alkylamines considering their large HOMO-LUMO gap,[47] and R_C and R_{SAM} are the contact resistance and SAM resistance, respectively.[48] We note that $T \propto e^{-\beta d}$ showing the relation with Equation (2). Equation (3) is valid for a junction with ideal point contacts (and R_c would be $1/G_0$ in an ideal case, where G_0 is the quantum conductance $2e^2/h$) and here it is only used to qualitatively discuss the impedance data.

$$R_{junction} = \frac{h}{2e^2M} + \frac{h}{2e^2M}\frac{1-T}{T} = R_C + R_{SAM} \quad (3)$$

Equation (3) shows that the R_C and R_{SAM} have to be added to each other to obtain $R_{junction}$ (at low frequencies when C_{SAM} is not important, e.g., in DC measurements) or in other words, R_C and R_{SAM} should be connected in series in the equivalent circuit. In AC experiments the C_{SAM} term dominates the impedance at high frequencies and has to be included in the equivalent circuit parallel to the R_{SAM}.[48,49] This equivalent circuit agrees with the mechanism of charge transport across the junction which is coherent tunneling (see **Figure 5**d) and the properties of the barrier are defined by the properties of the SAM and the SAM–electrode interfaces. Thus, the tunnel junction can be represented by the equivalent circuit shown in the inset of Figure 4a and is the same as the equivalent circuit used for *n*-alkanethiolate SAMs on noble metal electrodes.[12,46,49]

Figure 4b shows that R_C is independent of n. Previously, we have shown that R_C is dominated by the resistance of the SAM—electrode contacts.[12] Here the values of R_C range from 1.2–2.7 × 10^{-2} Ω cm^2, which is about 5 times higher than the contact resistance of Ag^{TS}-SC_n//GaO_x^{cond}/EGaIn junctions.[46] This increase in the interfacial resistance of our junctions is due to the presence of two van der Waals interfaces. The H_2NC_n SAMs form noncovalent contacts with both the top and bottom electrodes and result in a higher contact resistance R_C than alkanethiolate SAM based junctions that form metal—thiolate bonds with the bottom electrode that are more covalent in nature than the amine–graphene interaction. We note that the value of R_C is about 4 orders of magnitude smaller than the R_{SAM} for the shortest SAM (i.e., n = 8) and R_C is independent of the applied bias from which we conclude that the SAM//electrode interfaces behave as ohmic-like contacts with a very low resistance (at least in the bias range of ±1.0 V).

Figure 4b also shows that the value of R_{SAM} increases exponentially with n. R_{SAM} is given by Equation (4) where d_{SAM} is the SAM thickness and β_{SAM} is the decay coefficient.

$$R_{SAM} = R_{SAM,0}\, e^{\beta_{SAM} d_{SAM}} \quad (4)$$

The red solid line is a fit to Equation (4) resulting in $\beta = 0.95 \pm 0.03\ n_C^{-1}$, which is close to the value of β determined by DC methods as described above. Extrapolation of both R_{SAM} and R_C to $n = 0$ shows that R_C and $R_{SAM,0}$ are equal within one order of magnitude (and practically indistinguishable because of the long extrapolation), which further justifies the equivalent circuit.

As shown in Figure 4c, C_{SAM} is proportional to $1/d$ by following the parallel plate capacitance relation given by Equation (5) and the solid line is a fit to Equation (5), where ε_0 is the permittivity of vacuum, ε_r is the relative permittivity, A_{geo} is the geometrical contact area of the junction (1.9×10^3 μm^2 in our case), and d (determined by AFM, see Figure 2j) is the thickness of the SAM. This fit yields a value of $\varepsilon_r = 3.1 \pm 0.3$, which is consistent with previously reported values for junctions with organothiolate SAMs (2.7–3.4). [12,50]

$$C_{SAM} = \varepsilon_0 \varepsilon_r A_{geo}/d \quad (5)$$

To further probe the nature of the SAM–electrode interface, we performed potentiodynamic impedance spectroscopy on a junction with a SAM of H_2NC_{10} using the method established from alkanethiolate SAM-based junctions on silver. Figure 4e,f shows the dependence of the three equivalent circuit components on the applied DC bias. The SAM resistance R_{SAM} decreases exponentially with increasing DC bias as expected for a tunneling process.[51] The contact resistance R_C is independent of the applied DC bias suggesting all the noncovalent van der Waals interfaces (i.e., the Cu//graphene, graphene//H_2NC_n, and H_2NC_n//GaO_x^{cond}/EGaIn interfaces) are ohmic-like within the probed bias regime. In the case of nonohmic contacts such as a Schottky contact, the contact resistance changes with applied voltage as the contact barrier varies with applied voltage.[52] The SAM capacitance C_{SAM} is independent of the applied DC bias, indicating that charge trapping is not significant in the junctions. In the presence of significant charge trapping capacitance is altered by applying the voltage as the charge carriers can get excited from the traps due to the additional bias voltage.[52] Based on these findings, we conclude that the electrodes form low-resistance ohmic-like contacts to the SAMs and the mechanism of charge transport is determined by the molecular properties of the junctions instead of the contacts.

Stability Tests: To evaluate the stability of the noncovalent alkylamine SAM junctions on graphene, we studied their electrical stability against continuous cycling of voltage (1200 cycles), retention characteristics (over 100 000 s), aging in ambient conditions (297 K and 60%–65% relative humidity), and changes in temperature over the range of 100–340 K. All stability tests were carried out with PDMS confined microfluidic GaO_x^{cond}/EGaIn top electrodes and the results are summarized in Figure 5. Figure 5a shows the $J(V)$ curves taken over 1200 cycles (one cycle is 0 V→+1.0 V→−1.0 V→0 V) for three different junctions with $n = 8$, 12, and 16. Data for all junctions show stable electrical characteristics. The $J(V)$ curves of junction with $n = 16$ are more noisy than the others in the low-bias regime because the corresponding currents are low and close to the detection limit of the Keithley 6430 source meter we used. Figure 5b shows the retention characteristics of the three junctions measured at −1.0 V for 100 000 s by recording the current at intervals of 15 s. The values of $\log_{10}|J|$ within the retention time for the three junctions were −1.8 ± 0.5, −4.0 ± 0.4, and −5.5 ± 0.2 A cm^{-2}, respectively. The electrical characteristics of the junctions did not change significantly during the experiments, from which we conclude that they are electrically stable.

Aging of molecular junctions in ambient conditions has been rarely investigated. McCreery et al. showed that junctions with covalently bound monolayers can be stable for eight months.[53] Akkerman et al. showed that junctions of the form Au-SC_n//PEDOT:PSS did not change their electrical characteristics for 2.5 years[54] despite the fact that the Au—S bond is only stable for up to 1–2 d[5] and that PEDOT:PSS is permeable against O_2 and contains water.[55] These junctions[54] also have very low values of β and only show molecular effects when $n > 12$ implying that the top-electrode intercalates with, or partially displaces, the SAMs. We showed that junctions of the form Ag^{TS}-SC_n//GaO_x^{cond}/EGaIn are stable for 2–3 days after which the values of J decrease by a factor of 10 over a period of one week which we attributed to the instability of the metal—thiolate bond.[3]

Figure 5c shows the $J(V)$ curves of Cu//Graphene//H_2NC_n//GaO_x^{cond}/EGaIn junctions with $n = 12$ and 16 measured over a period of 29–35 d. Similar measurements for junctions with $n = 8$, 10, and 14 are shown in Figure S14a–c, Supporting Information. The current density of the junction with $n = 8$ decreased by a factor of 10 within 8 d, so we did not continue the aging process with this junction. The current density of junctions with $n = 10$ and 12 decreases by a factor about 10 and 5 within 30 d, respectively, while for junctions with $n = 14$ and 16, the current density did not show significant decay within 35 d. The Cu//Graphene//H_2NC_n//GaO_x^{cond}/EGaIn junctions are stable for the following reasons. First, the Graphene//$H_2N(CH_2)_{n-1}CH_3$ contact is chemically stable in ambient conditions. Second, the layer of graphene effectively protects the Cu from oxidation because graphene is impermeable to O_2.[23] Third, the highly conductive native layer of GaO_x is self-limiting and protects the bulk liquid metal from oxidation. In our experiments, we observed that the stability of the junctions improved with the increase of chain length, which can be ascribed to the length-dependent SAM packing energy (Figure 2i) and an increase of the melting point of the alkylamines.[56] The junctions with SAMs of H_2NC_8 show quick decay because of the small packing energy (Figure 2i) and low melting point of the H_2NC_8 molecules (−1 °C).[56] These SAMs may not remain stable against evaporation at room temperature over the investigated periods of time. In contrast, H_2NC_n with $n \geq 10$ have higher melting points (>12 °C)[56] and SAM packing energies greater than 20 kcal mol^{-1}, and are stable over extended periods of time (we did not investigate their stability beyond 35 d). We believe that the increase of SAM packing energy and melting points for longer molecules account for their increasing electrical stability under ambient conditions.

Temperature dependent $J(V)$ measurements were used to determine the mechanism of charge transport. We performed $J(V,T)$ measurements over a range of temperatures of 100–340 K. Figure 5d shows that the $J(V)$ traces are independent of T from

which we conclude that the mechanism of charge transport across the junctions is coherent tunneling.

In summary, our results show that noncovalent H_2NC_n SAMs on graphene form a good barrier against tunneling in SAM-based junctions with GaO_x^{cond}/EGaIn top contacts and have electrical characteristics comparable to similar junctions based on organothiolate SAMs on gold and silver. The independence of the $J(V)$ curves over a broad range of temperatures (100–340 K), the value of $\beta = 1.02 \pm 0.08\ n_C^{-1}$ and the linearity of the $J(V)$ curves in the low-bias regime (±0.10 V) indicate that the mechanism of charge transport is coherent through-bond tunneling. Impedance spectroscopy revealed that the SAM resistance increases exponentially with increasing chain length and dominates the charge transport properties of the junctions; the SAM–electrode interfaces behave as ohmic-like contacts with a very low resistance within the measured bias range of ±1.0 V and is a factor of 10^4 smaller than the resistance of the thinnest SAM of H_2NC_8. The junctions are electrically stable and they did not change their electrical characteristics over a period of more than 30 d in ambient conditions, while organothiolate —metal bonds are only stable for 1–2 d.[3] We believe that our method could also be useful to incorporate other types of 2D materials in molecular junctions, and in principle the alkylamines can be functionalized with redox-, light-, or magnetic-responsive groups interacting with the 2D material, paving the way to new types of molecular electronic junctions.

Supporting Information

Supporting Information is available from the Wiley Online Library or from the author.

Acknowledgements

The National Research Foundation (NRF) is kindly acknowledged for supporting this research under the CRP program (Award no. NRF-CRP 8-2011-07). Prime Minister's Office, Singapore under its Medium sized center program is also acknowledged for supporting this research. D.T. acknowledges Science Foundation Ireland (SFI) for financial support under Grant No. 11/SIRG/B2111 and computing resources at the SFI/Higher Education Authority Irish Centre for High-End Computing (ICHEC). We also would like to thank Enrique Del Barco for the very insightful discussions.

Received: August 28, 2015
Revised: October 2, 2015
Published online: November 30, 2015

[1] a) R. L. McCreery, *Chem. Mater.* **2004**, *16*, 4477; b) H. Haick, D. Cahen, *Acc. Chem. Res.* **2008**, *41*, 359; c) A. Vilan, O. Yaffe, A. Biller, A. Salomon, A. Kahn, D. Cahen, *Adv. Mater.* **2010**, *22*, 140.
[2] G. Wang, T.-W. Kim, T. Lee, *J. Mater. Chem.* **2011**, *21*, 18117.
[3] A. Wan, L. Jiang, C. S. S. Sangeeth, C. A. Nijhuis, *Adv. Funct. Mater.* **2014**, *24*, 4442.
[4] L. Yuan, L. Jiang, B. Zhang, C. A. Nijhuis, *Angew. Chem. Int. Ed.* **2014**, *53*, 3377.
[5] J. C. Love, L. A. Estroff, J. K. Kriebel, R. G. Nuzzo, G. M. Whitesides, *Chem. Rev.* **2005**, *105*, 1103.
[6] a) Y. S. Cohen, A. Vilan, I. Ron, D. Cahen, *J. Phys. Chem. C* **2009**, *113*, 6174; b) Y. Li, S. Calder, O. Yaffe, D. Cahen, H. Haick, L. Kronik, H. Zuilhof, *Langmuir* **2012**, *28*, 9920.
[7] I. Levine, S. M. Weber, Y. Feldman, T. Bendikov, H. Cohen, D. Cahen, A. Vilan, *Langmuir* **2012**, *28*, 404.
[8] H. Yan, A. J. Bergren, R. L. McCreery, *J. Am. Chem. Soc.* **2011**, *133*, 19168.
[9] J. Ru, B. Szeto, A. Bonifas, R. L. McCreery, *ACS Appl. Mater. Interfaces* **2010**, *2*, 3693.
[10] S. Onclin, B. J. Ravoo, D. N. Reinhoudt, *Angew. Chem. Int. Ed.* **2005**, *44*, 6282.
[11] R. C. Chiechi, E. A. Weiss, M. D. Dickey, G. M. Whitesides, *Angew. Chem. Int. Ed.* **2008**, *47*, 142.
[12] C. S. S. Sangeeth, A. Wan, C. A. Nijhuis, *J. Am. Chem. Soc.* **2014**, *136*, 11134.
[13] a) W. F. Reus, M. M. Thuo, N. D. Shapiro, C. A. Nijhuis, G. M. Whitesides, *ACS Nano* **2012**, *6*, 4806; b) L. Cademartiri, M. M. Thuo, C. A. Nijhuis, W. F. Reus, S. Tricard, J. R. Barber, R. N. S. Sodhi, P. Brodersen, C. Kim, R. C. Chiechi, G. M. Whitesides, *J. Phys. Chem. C* **2012**, *116*, 10848.
[14] M. M. Thuo, W. F. Reus, C. A. Nijhuis, J. R. Barber, C. Kim, M. D. Schulz, G. M. Whitesides, *J. Am. Chem. Soc.* **2011**, *133*, 2962.
[15] N. Nerngchamnong, L. Yuan, D.-C. Qi, J. Li, D. Thompson, C. A. Nijhuis, *Nat. Nanotechnol.* **2013**, *8*, 113.
[16] C. A. Nijhuis, W. F. Reus, J. R. Barber, G. M. Whitesides, *J. Phys. Chem. C* **2012**, *116*, 14139.
[17] E. A. Weiss, R. C. Chiechi, G. K. Kaufman, J. K. Kriebel, Z. Li, M. Duati, M. A. Rampi, G. M. Whitesides, *J. Am. Chem. Soc.* **2007**, *129*, 4336.
[18] H. Y. Nan, Z. H. Ni, J. Wang, Z. Zafar, Z. X. Shi, Y. Y. Wang, *J. Raman Spectrosc.* **2013**, *44*, 1018.
[19] X. Li, W. Cai, J. An, S. Kim, J. Nah, D. Yang, R. Piner, A. Velamakanni, I. Jung, E. Tutuc, S. K. Banerjee, L. Colombo, R. S. Ruoff, *Science* **2009**, *324*, 1312.
[20] B. Long, M. Manning, M. Burke, B. N. Szafranek, G. Visimberga, D. Thompson, J. C. Greer, I. M. Povey, J. MacHale, G. Lejosne, D. Neumaier, A. J. Quinn, *Adv. Funct. Mater.* **2012**, *22*, 717.
[21] S. O'Mahony, C. O'Dwyer, C. A. Nijhuis, J. C. Greer, A. J. Quinn, D. Thompson, *Langmuir* **2013**, *29*, 7271.
[22] S. Seo, M. Min, S. M. Lee, H. Lee, *Nat. Commun.* **2013**, *4*, 1920.
[23] S. Chen, L. Brown, M. Levendorf, W. Cai, S.-Y. Ju, J. Edgeworth, X. Li, C. W. Magnuson, A. Velamakanni, R. D. Piner, J. Kang, J. Park, R. S. Ruoff, *ACS Nano* **2011**, *5*, 1321.
[24] C. P. Y. Wong, T. J. H. Koek, Y. Liu, K. P. Loh, K. E. J. Goh, C. Troadec, C. A. Nijhuis, *ACS Appl. Mater. Interfaces* **2014**, *6*, 20464.
[25] J. W. Suk, W. H. Lee, J. Lee, H. Chou, R. D. Piner, Y. Hao, D. Akinwande, R. S. Ruoff, *Nano Lett.* **2013**, *13*, 1462.
[26] a) L. Gao, G.-X. Ni, Y. Liu, B. Liu, A. H. Castro Neto, K. P. Loh, *Nature* **2014**, *505*, 190; b) Y. Wang, Y. Zheng, X. Xu, E. Dubuisson, Q. Bao, J. Lu, K. P. Loh, *ACS Nano* **2011**, *5*, 9927.
[27] C.-F. Chen, C.-H. Park, B. W. Boudouris, J. Horng, B. Geng, C. Girit, A. Zettl, M. F. Crommie, R. A. Segalman, S. G. Louie, F. Wang, *Nature* **2011**, *471*, 617.
[28] a) Y. Kim, J. Park, J. Kang, J. M. Yoo, K. Choi, E. S. Kim, J.-B. Choi, C. Hwang, K. S. Novoselov, B. H. Hong, *Nanoscale* **2014**, *6*, 9545; b) A. C. Crowther, A. Ghassaei, N. Jung, L. E. Brus, *ACS Nano* **2012**, *6*, 1865.
[29] P. Harder, M. Grunze, R. Dahint, G. M. Whitesides, P. E. Laibinis, *J. Phys. Chem. B* **1998**, *102*, 426.
[30] P. E. Laibinis, R. G. Nuzzo, G. M. Whitesides, *J. Phys. Chem.* **1992**, *96*, 5097.
[31] I. V. Chernyshova, K. H. Rao, A. Vidyadhar, A. V. Shchukarev, *Langmuir* **2000**, *16*, 8071.

[32] J. J. Benitez, M. A. San-Miguel, S. Dominguez-Meister, J. A. Heredia-Guerrero, M. Salmeron, *J. Phys. Chem. C* **2011**, *115*, 19716.
[33] J. C. Love, D. B. Wolfe, R. Haasch, M. L. Chabinyc, K. E. Paul, G. M. Whitesides, R. G. Nuzzo, *J. Am. Chem. Soc.* **2003**, *125*, 2597.
[34] R. Chang, J. Lee, *Bull. Korean Chem. Soc.* **2010**, *31*, 3195.
[35] C. L. Apel, D. W. Deamer, M. N. Mautner, *BBA-Biomembranes* **2002**, *1559*, 1.
[36] G. Giovannetti, P. A. Khomyakov, G. Brocks, V. M. Karpan, J. van den Brink, P. J. Kelly, *Phys. Rev. Lett.* **2008**, *101*, 026803.
[37] W. F. Reus, C. A. Nijhuis, J. R. Barber, M. M. Thuo, S. Tricard, G. M. Whitesides, *J. Phys. Chem. C* **2012**, *116*, 6714.
[38] L. Jiang, C. S. S. Sangeeth, A. Wan, A. Vilan, C. A. Nijhuis, *J. Phys. Chem. C* **2015**, *119*, 960.
[39] F. C. Simeone, H. J. Yoon, M. M. Thuo, J. R. Barber, B. Smith, G. M. Whitesides, *J. Am. Chem. Soc.* **2013**, *135*, 18131.
[40] F. Milani, C. Grave, V. Ferri, P. Samorì, M. A. Rampi, *ChemPhysChem* **2007**, *8*, 515.
[41] H. B. Akkerman, P. W. M. Blom, D. M. de Leeuw, B. de Boer, *Nature* **2006**, *441*, 69.
[42] K. Slowinski, R. V. Chamberlain, C. J. Miller, M. Majda, *J. Am. Chem. Soc.* **1997**, *119*, 11910.
[43] Y. Selzer, A. Salomon, D. Cahen, *J. Phys. Chem. B* **2002**, *106*, 10432.
[44] X. D. Cui, X. Zarate, J. Tomfohr, O. F. Sankey, A. Primak, A. L. Moore, T. A. Moore, D. Gust, G. Harris, S. M. Lindsay, *Nanotechnology* **2002**, *13*, 5.
[45] J. R. Macdonald, W. B. Johnson, *Impedance Spectroscopy*, John Wiley & Sons, Inc. Hoboken, NJ **2005**, p. 1.
[46] C. S. Suchand Sangeeth, A. Wan, C. A. Nijhuis, *Nanoscale* **2015**, *7*, 12061.
[47] J. Heurich, J. C. Cuevas, W. Wenzel, G. Schön, *Phys. Rev. Lett.* **2002**, *88*, 256803.
[48] S. Datta, *Electronic Transport in Mesoscopic Systems*, Cambridge University Press, Cambridge **1995**.
[49] H. B. Akkerman, R. C. G. Naber, B. Jongbloed, P. A. van Hal, P. W. M. Blom, D. M. de Leeuw, B. de Boer, *Proc. Natl. Acad. Sci. U.S.A.* **2007**, *104*, 11161.
[50] M. A. Rampi, O. J. A. Schueller, G. M. Whitesides, *Appl. Phys. Lett.* **1998**, *72*, 1781.
[51] J. M. Beebe, V. B. Engelkes, L. L. Miller, C. D. Frisbie, *J. Am. Chem. Soc.* **2002**, *124*, 11268.
[52] S. M. Sze, K. K. Ng, *Physics of Semiconductor Devices*, John Wiley & Sons, Inc. **2006**, p. 134.
[53] S. Y. Sayed, A. Bayat, M. Kondratenko, Y. Leroux, P. Hapiot, R. L. McCreery, *J. Am. Chem. Soc.* **2013**, *135*, 12972.
[54] H. B. Akkerman, A. J. Kronemeijer, J. Harkema, P. A. van Hal, E. C. P. Smits, D. M. de Leeuw, P. W. M. Blom, *Org. Electron.* **2010**, *11*, 146.
[55] K. Norrman, M. V. Madsen, S. A. Gevorgyan, F. C. Krebs, *J. Am. Chem. Soc.* **2010**, *132*, 16883.
[56] S. A. Lawrence, in *Amines: Synthesis, Properties and Applications*, Cambridge University Press, Cambridge **2004**.